Inorganic Chemistry Communications 188 (2026) 116457

Contents lists available at ScienceDirect

Inorganic Chemistry Communications

journal homepage: www.elsevier.com/locate/inoche

Research Article

The performance of phthalocyanine-based catalysts for photocatalytic degradation of chlorophenols

Cagla Akkol [a,b], Ece Tugba Saka [a,*], Ahmet Senocak [c]

[a] Karadeniz Technical University, Faculty of Science, Department of Chemistry, 61080 Trabzon, Türkiye
[b] Karadeniz Technical University, Institue of Science, Department of Chemistry, 61080 Trabzon, Türkiye
[c] Department of Chemistry, Faculty of Science, Gebze Technical University, 41400 Gebze, Turkey

ARTICLE INFO

Keywords:
Phthalocyanine
Graphitic carbon nitride
Phenol degradation
Photocatalysis

ABSTRACT

The degradation of chlorophenols is crucial to remove toxic, persistent, and bioaccumulative pollutants from the environment, protect ecosystems and human health, and enable sustainable pollution management through bioremediation and green chemistry. In this study, 2(3), 9(10), 16(17), 23(24)-Tetrakis-[ethyl (E)-3-[4-(phenoxy)phenyl]acrylate phthalocyaninato copper (II) (EpA-CuPc) and 2(3), 9(10), 16(17), 23(24)-Tetrakis-[ethyl (E)-3-[4-(phenoxy)phenyl]acrylate phthalocyaninato cobalt (II) (EpA-CoPc) were synthesized and characterized with different spectral techniques (FT-IR, UV–Vis and Mass) to undergo π-π interaction with graphitic carbon nitride to produce an effective catalyst. Two effective catalysts' structure were identified with FT-IR, SEM, XRD and BET then, their photocatalytic performances, recycling works in 2-chlorophenol, 2,3-dichlorophenol, and 2,3,6-trimethyl phenol degradation were examined. The optimum catalyst loading for the MPc/g-C_3N_4 composites was determined as 0.5 g/L, providing the highest photocatalytic efficiency. The EpCA-CoPc/g-C_3N_4 catalyst achieved 93.2% product selectivity and 85.8% conversion in the oxidation of 2-chlorophenol, while the EpCA-CuPc/g-C_3N_4 catalyst achieved approximately 87% removal. The conversion order of the pollutants was 2-CP > 2,3-DCP > 2,3,6-TCP, with benzoquinone derivatives identified as the major oxidation products. In recycling tests, both catalysts retained more than 50% of their activity after five cycles; EpCA-CoPc/g-C_3N_4 reached 65% conversion after the 4th cycle, and EpCA-CuPc/g-C_3N_4 reached 63% after the 3rd cycle.

1. Introduction

The rapid expansion of global industrial activities has resulted in the substantial accumulation of phenolic compounds in aquatic environments, presenting severe threats to both ecological integrity and public health. Among these pollutants, chlorophenols (CPs) are particularly notorious for their acute toxicity, chemical recalcitrance, and bioaccumulative nature. Despite the existence of conventional treatment methods, the degradation of multi-chlorinated phenols remains a formidable challenge due to their stable carbon-chlorine bonds, necessitating the urgent development of next-generation advanced oxidation processes (AOPs) that are both energy-efficient and environmentally sustainable [1–5].

In recent years, photocatalysis has emerged as a frontline technology for organic pollutant remediation, with graphitic carbon nitride (g-C_3N_4) garnering significant attention as a metal-free, visible-light-active semiconductor. However, the current research landscape indicates that the practical application of pristine g-C_3N_4 is severely hampered by its inherent limitations, such as a low specific surface area and the rapid recombination of photo-generated electron-hole pairs. To overcome these barriers, recent progress has shifted toward the molecular hybridization of g-C_3N_4 with macrocyclic complexes, particularly metallophthalocyanines (MPcs). These complexes serve as exceptional sensitizers that not only extend the light-harvesting window of g-C_3N_4 deep into the visible region but also facilitate superior charge separation through non-covalent π-π stacking interactions [6–13].

A photocatalyst is typically a semiconductor material capable of initiating redox reactions under light irradiation. When exposed to light, it generates oxidative and reductive sites on its surface, enabling electron transfer [14,15].For electrical conductivity to occur, electrons must be excited from the valence band to the conduction band. In semiconductors, this bandgap is relatively narrow, allowing the excited electrons to migrate efficiently between the two bands. Such electron transitions can be induced by external stimuli, including light, heat, or

* Corresponding author.
E-mail address: esaka@ktu.edu.tr (E.T. Saka).

https://doi.org/10.1016/j.inoche.2026.116457
Received 21 November 2025; Received in revised form 11 February 2026; Accepted 4 March 2026
Available online 8 March 2026
1387-7003/© 2026 Elsevier B.V. All rights are reserved, including those for text and data mining, AI training, and similar technologies.

an applied electric field [16–18]. Despite these advancements, a critical gap remains in the development of photocatalysts that combine high textural porosity with biologically inspired molecular designs. In this work, ethyl p-coumarate (EpCA) groups substituted Co(II) and Cu(II) phthalocyanine were synthesized and characterized at the first step. EpCA is widely known to be strong antioxidant, antimicrobial, antifungal and antiradical activity [19]. This work presents an innovative approach that addresses critical gaps in existing literature by utilizing ethyl p-coumarate (EpCA) substituted phthalocyanines, which differ from the simpler sulfonyl or carboxyl substituents commonly found in previous methods. While traditional strategies often rely on harsh covalent grafting, this approach employs non-covalent π-π stacking interactions between the π-electron-rich peripheral groups and graphitic carbon nitride (g-C_3N_4), allowing for better structural tunability and sustainability. By combining the catalytic activity of redox active metal-centered phthalocyanines with the broad light absorption properties of graphitic carbon nitride, optimum conditions for photocatalytic degradation of chlorophenols were determined.

2. Experimental

2.1. Materials

All materials, equipment, general procedures of EpCA-CN, EpCA-CoPc, EpCA-CuPc, g-C_3N_4, EpCA-CoPc/g-C_3N_4, EpCA-CuPc/g-C_3N_4, photocatalytic procedure and the details of the free radical scavenging experiments are given as Supplementary file. The ground-state geometries and excited-state properties (gas-phase TD-DFT) of phthalocyanine derivatives (CoPc and CuPc) are presented in Supplementary file.

2.2. Synthesis

2.2.1. Synthesis of ethyl (2Z)-3-(4-(3,4-dicyanophenoxy)phenyl)acrylate (EpCA-CN)

Yield: 2.64 g (80%); FT-IR: υmax /cm^{-1} 3000–3100 (Ar—H), 2950–2850 (Alif. C—H), 2227 (C≡N),1704 (C=O), 1586, 1504, 1488, 1416,1370,1300, 1280, 1252, 1213, 1174 (ArC–O) 974, 957, 894, 769, 622. ^{1}H NMR. (DMSO), (d:ppm): 8.13 (d, *J*:8.8, H, Ar—H), 7.87 (d, *J*:8.8, 3H, Ar—H),7.84 (s, H, Ar—H), 7.71 (d, *J*:8.0, H, Ar—H), 7.49 (d, *J*:6.0, 2H, CH═CH), 6.66 (d, *J*:8.4, H, Ar—H), 4.23–4.11 (q, *J*:7.2, 2H, CH2-O), 1.28 (t, *J*:6.8, 3H, CH3). ^{13}C NMR. (DMSO), (d:ppm): 166.66 (C_3), 160.78 (C_{12}), 156.12 (C_9), 143.72 (C_4), 136.83 (C_{14}), 131.90 (C_{11}-C_7), 131.20 (C_{12}), 123.81 (C_6), 123.26 (C_{17}), 120.82 (C_{13}), 118.68 (C_{16}), 117.27 (C_{10}-C_8), 116.32 (C_{18}), 115.32 (C_{19}), 109.27 (C_{15}), 60.54 (C_2), 14.67 (C_1). MALDI-TOF-MS: *m/z*: calcd. 318.32; found 318.04 [M]+, 356.56 [M + K-H]+, 381.895 [M + 2 K-CH3].

2.2.2. Co(II) phthalocyanine (EpCA-CoPc)

The green solid product had good solubility in THF, DMF, DMSO and $CHCl_3$ solvents. Yield: 280 mg(%45); FT-IR: υmax /cm^{-1} 3030–3003 (Ar—H), 2953–2929-2859 (Alif. C—H), 1706 (C=O), 1595, 1504, 1465, 1407, 1322, 1229–1230–1158–1117 (ArC–O) 1091, 1055, 1012, 977, 955, 876,824, 750. UV/Vis (DMSO): λ_{max} (log ε) 671 (4.37), 606 (3.88), 300 (4.47).MALDI-TOF-MS: *m/z*: m/z: calcd. 1332.21; found 1334.64 $[M + 2H]^+$.

2.2.3. Cu(II) phthalocyanine (EpCA-CuPc)

The green solid product had good solubility in THF, DMF, DMSO, and $CHCl_3$ solvents. Yield: 300 mg(%50); FT-IR: υmax /cm^{-1} 3035–3003 (Ar—H), 2975–2932-2901 (Alif. C—H), 1704 (C=O), 1596, 1503, 1464,1398, 1311, 1227–1156–1087 (ArC–O) 1045, 977, 948, 822,744. UV/Vis (DMSO): λ_{max} (log ε) 680 (4.69), 613 (4.19), 418 (3.86). MALDI-TOF-MS: *m/z*: m/z: calcd. 1336.82; found 1336.51 $[M]^+$.

3. Results and discussion

3.1. Synthesis and characterization

All synthetic pathways were given in Fig. 1. EpCA-CN was successfully synthesized and its structure was verified by FT-IR, NMR and Mass spectral techniques. In the FT-IR spectrum, the sharp absorption at 2227 cm^{-1} corresponds to the C≡N stretching vibration of the dicyano group, while the strong band at 1704 cm^{-1} confirms the ester C═O group. The characteristic aromatic (3000–3100 cm^{-1}) and aliphatic (2950–2850 cm^{-1}) C—H vibrations were also evident. The ^{1}H NMR spectrum exhibited multiple aromatic proton signals between 7.4 and 8.1 ppm, confirming the presence of phenyl and phenoxy moieties (*Supplementary Fig. 1*). The signal at 6.66 ppm is attributed to the CH═CH protons of the conjugated acrylate group, the quartet at 4.11–4.23 ppm (CH_2–O) and the triplet at 1.28 ppm (CH_3) correspond to the ethyl ester moiety. In ^{13}C NMR spectrum, the resonance at 166.66 ppm is assigned to the ester carbonyl carbon, while the signals between 115 and 120 ppm correspond to the cyano carbons (*Supplementary Fig. 2*). MALDI-TOF-MS analysis showed a molecular ion peak at *m/z* = 318.04 $[M]^+$, consistent with the calculated value (318.32 g/mol), confirming the successful formation of EpCA-CN (*Supplementary Fig. 3*).

FT-IR spectrum revealed the retention of the C═O stretching at 1706 cm^{-1} for EpCA-CoPc and 1704 cm^{-1} for EpCA-CuPc. The aromatic C—O stretching bands at 1229–1117 cm^{-1}, indicating that the EpCA moiety was successfully incorporated into the phthalocyanine framework and the disappearance of the C≡N band verified the completion of the cyclotetramerization reaction, forming the phthalocyanine macrocycle. The UV–Vis spectrum displayed intense Q-bands at 671 and 606 nm and a B (Soret) band at 300 nm, characteristic of metal phthalocyanines for EpCA-CoPc (*Supplementary Fig. 4*). The slight splitting and bathochromic shift of Q-bands are consistent with a D4h-symmetric Co(II) phthalocyanine structure and the paramagnetic nature of the Co^{2+} center. The MALDI-TOF-MS peak at *m/z* = 1440.53 $[M + DIT+K]^+$ further confirmed molecular structure of EpCA-CoPc (*Supplementary Fig. 5 A*). Similarly, UV–Vis spectrum of EpCA-CuPc showed Q-bands at 680 and 613 nm and a B-band at 418 nm, all characteristic of Cu(II) phthalocyanines (*Supplementary Fig. 4*). Compared with the CoPc analog, the CuPc complex exhibited a red-shifted Q-band (680 nm) and higher molar absorptivity (log ε = 4.69), indicating stronger π–π* delocalization and enhanced visible-light absorption due to the diamagnetic Cu^{2+} center. The MALDI-TOF-MS peak at *m/z* = 1336.82 $[M]^+$ further confirmed molecular structure of EpCA-CoPc (*Supplementary Fig. 5B*).

The structural interactions between phthalocyanine (MPc) and g-C_3N_4 were confirmed by FT-IR, XRD, SEM and BET analyses, these techniques provided clear evidence of π–π stacking between the two components. In the FT-IR spectra, the characteristic bands of g-C_3N_4 appeared at around 810 cm^{-1} (triazine ring breathing) and in the 1200–1650 cm^{-1} region (C—N and C═N stretching), indicating that the basic framework of g-C_3N_4 remained intact after composite formation. However, slight red shifts of the C–N/C=N vibrations and the weakening of the broad N—H stretching band (3100–3300 cm^{-1}) were observed, suggesting strong π–π interactions and possible hydrogen bonding between the aromatic π-systems of MPc and g-C_3N_4 (Fig. 2A). In addition, the retention of MPc-related C═O and Ar–C–O bands confirmed the successful incorporation of the phthalocyanine moiety onto the g-C_3N_4 surface.XRD patterns further supported these findings: pristine g-C_3N_4 exhibited two major diffraction peaks at 13.1° and 27.4° corresponding to in-plane structural packing and interlayer stacking of the conjugated layers. After MPc loading, the peak slightly shifted toward lower angles (≈27.0°) and decreased in intensity, indicating an increased interlayer spacing due to MPc insertion and a partial disturbance of the ordered stacking structure. The reflection also broadened slightly, suggesting reduced in-plane crystallinity caused by MPc–g-C_3N_4 interaction. Together, the FT-IR and XRD results confirm that MPc molecules are effectively anchored onto g-C_3N_4 through noncovalent π–π stacking

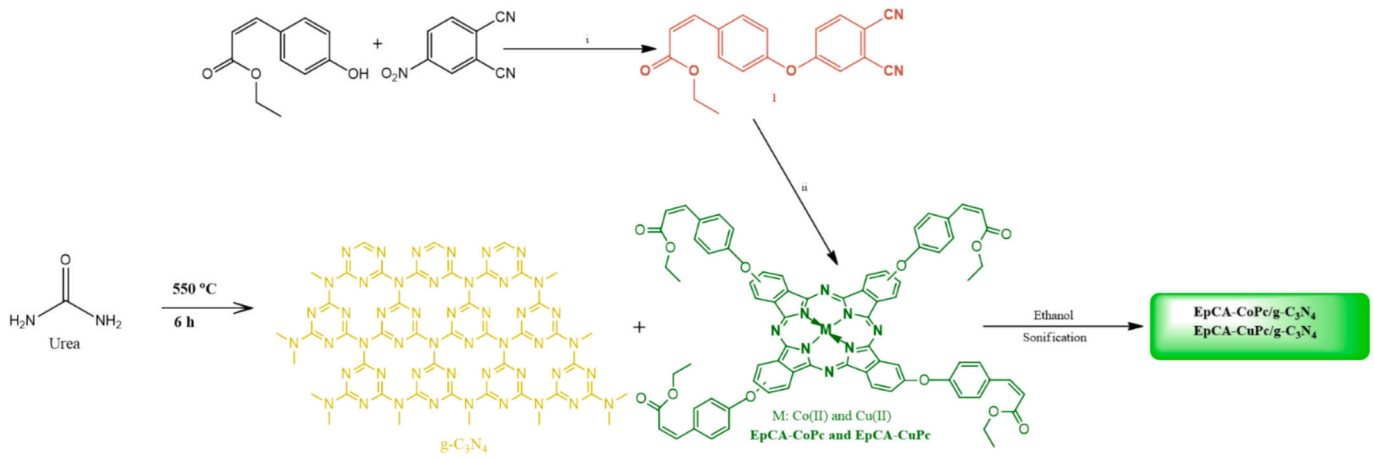


Fig. 1. Schematic illustration of the synthetic pathways for the preparation of the target molecules and metallophthalocyanine/graphitic carbon nitride composites. (i) K_2CO_3, DMF, 50 °C, 72 h; (ii) *n*-pentanol, DBU, $CoCl_2$ or $CuCl_2$, 160 °C, 24 h.

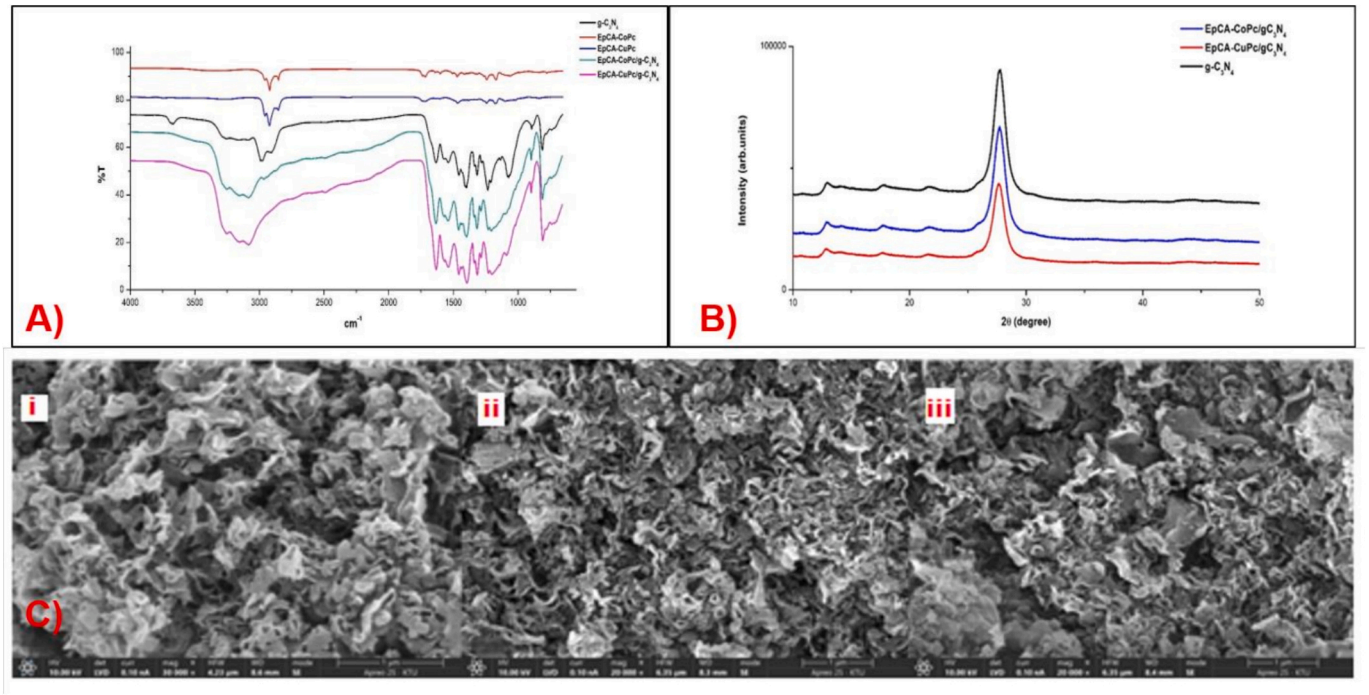


Fig. 2. A) FT-IR spectra of g-C_3N_4, EpCA-CoPc, EpCA-CuPc, EpCA-CoPc/g-C_3N_4 and EpCA-CuPc/g-C_3N_4·B) XRD spectra of EpCA-CoPc/g-C_3N_4 and EpCA-CuPc/g-C_3N_4 and g-C_3N_4, C)SEM images of i: g-C_3N_4 ii: EpCA-CoPc/ g-C_3N_4 iii: EpCA-CuPc/ g-C_3N_4.

interactions, enhancing charge transfer pathways and creating a stable hybrid interface beneficial for photocatalytic activity (Fig. 2B). Fig. 2C(i-iii) shows the images of g-C_3N_4, EpCA-CoPc/g-C_3N_4, EpCA-CuPc/g-C_3N_4 to prove noncovalent π–π stacking interactions between metallophthalocyanines and g-C_3N_4.

Nitrogen adsorption–desorption analyses were performed to comparatively evaluate the textural properties of pristine g-C_3N_4 and metal phthalocyanine–modified samples (EpCA-CoPc/g-C_3N_4 and EpCA-CuPc/g-C_3N_4). Pristine g-C_3N_4 exhibited a relatively low BET surface area of 15.41 $m^2\ g^{-1}$ and a total pore volume of 0.043 $cm^3\ g^{-1}$, which can be attributed to its intrinsically stacked layered structure (Fig. 3). Upon EpCA-CoPc incorporation, a marked increase in BET surface area to 23.27 $m^2\ g^{-1}$ was observed, together with a substantial rise in pore volume (0.067 $cm^3\ g^{-1}$), indicating the development of a more open and accessible mesoporous architecture. In comparison, EpCA-CuPc modified sample displayed an intermediate surface area of 19.08 $m^2\ g^{-1}$ and a pore volume of 0.045 $cm^3\ g^{-1}$, suggesting that EpCA-CuPc incorporation partially disrupts the interlayer stacking of g-C_3N_4, albeit less effectively than EpCA-CoPc. Overall, EpCA-CoPc modification appears to be more effective in tailoring the textural properties of g-C_3N_4, a feature that is expected to be advantageous for catalytic applications by enhancing mass transport and increasing the accessibility of active sites. From a catalytic and photocatalytic perspective, the observed differences in surface area and pore structure are expected to play a crucial role in governing the overall activity of the materials. The higher BET surface area and enlarged mesoporous volume of the EpCA-CoPc modified g-C_3N_4 provide a greater number of accessible surface sites, which can facilitate the uniform dispersion of catalytically active EpCA-CoPc species and enhance reactant adsorption. Moreover, the well-developed mesoporosity is beneficial for mass transport, reducing diffusion limitations and promoting efficient charge transfer at the solid–liquid or solid–gas interface. In contrast, the relatively lower surface

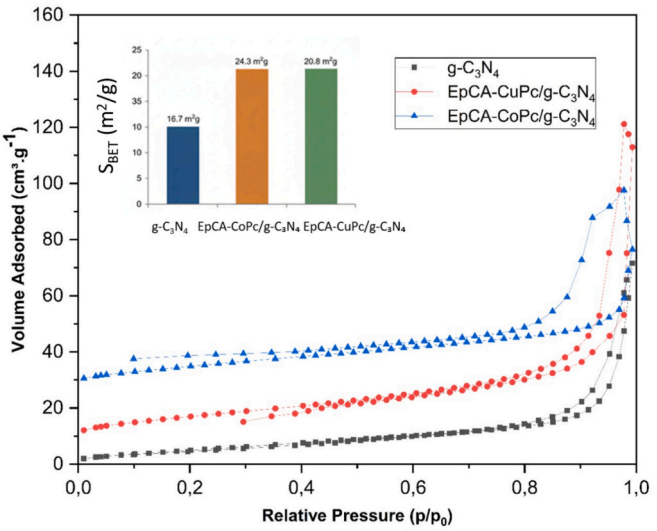


Fig. 3. Nitrogen adsorption-desorption isotherms of g-C_3N_4, EpCA-CoPc/g-C_3N_4 and EpCA-CuPc/g-C_3N_4 with the inset displaying the calculated BET surface areas.

area and pore volume of pristine g-C_3N_4 may restrict the availability of active sites and slow reactant diffusion, thereby limiting its catalytic efficiency. Although EpCA-CuPc modified sample shows moderate textural improvement, its comparatively lower mesopore volume suggests a less pronounced contribution to mass-transfer enhancement. Consequently, the superior textural properties induced by EpCA-CoPc incorporation are anticipated to synergistically improve catalytic and photocatalytic performance by increasing active site exposure, facilitating reactant accessibility, and supporting more efficient utilization of photogenerated charge carriers.

3.2. Photocatalytical studies

The photocatalytic performance of MPc/g-C_3N_4 composites in the degradation of chlorophenols is highly dependent on the catalyst loading, which directly affects the availability of active sites and light absorption efficiency. At low loadings, the limited number of photocatalyst particles reduces the formation of photogenerated electron-hole pairs, leading to suboptimal production of reactive oxygen species such as hydroxyl (•OH) and superoxide ($O_2^{\bullet-}$) radicals, thus slowing down pollutant degradation. Conversely, excessively high catalyst loadings can cause light scattering and shielding effects, where the upper layers of particles block incident light from reaching deeper layers, reducing overall photon absorption. Furthermore, high loading can lead to agglomeration of MPc/g-C_3N_4 particles, reducing the effective surface area for pollutant adsorption and radical generation. Optimum loading balances these effects, ensuring sufficient surface area, maximum light utilization, and efficient production of reactive radicals, thus achieving the highest photocatalytic degradation rates. Literature studies for MPc/g-C_3N_4 systems generally include optimum loadings in the range of 0.5–2.0 g/L; however, the exact value depends on the specific MPc species, g-C_3N_4 morphology, light intensity, and target pollutant concentration [20–22]. In this study, loadings in the range of 0.5–2.0 g/L were performed (Fig. 4A) and the optimum loading was determined to be 0.5 g/L for both photocatalysts (25 mg of phthalocyanine in 50 mL ethanol).

The ease with which phenol derivatives undergo oxidation can vary depending on the effects of electron-withdrawing or repulsive groups on the aromatic ring. The oxidation products of 2-chlorophenol, 2,3-dichlorophenol, and 2,3,6-trichlorophenol used in this study were identified as benzoquinone derivatives (Table 1). Chlorine acts as a highly electronegative atom that exerts a strong inductive effect (—I),

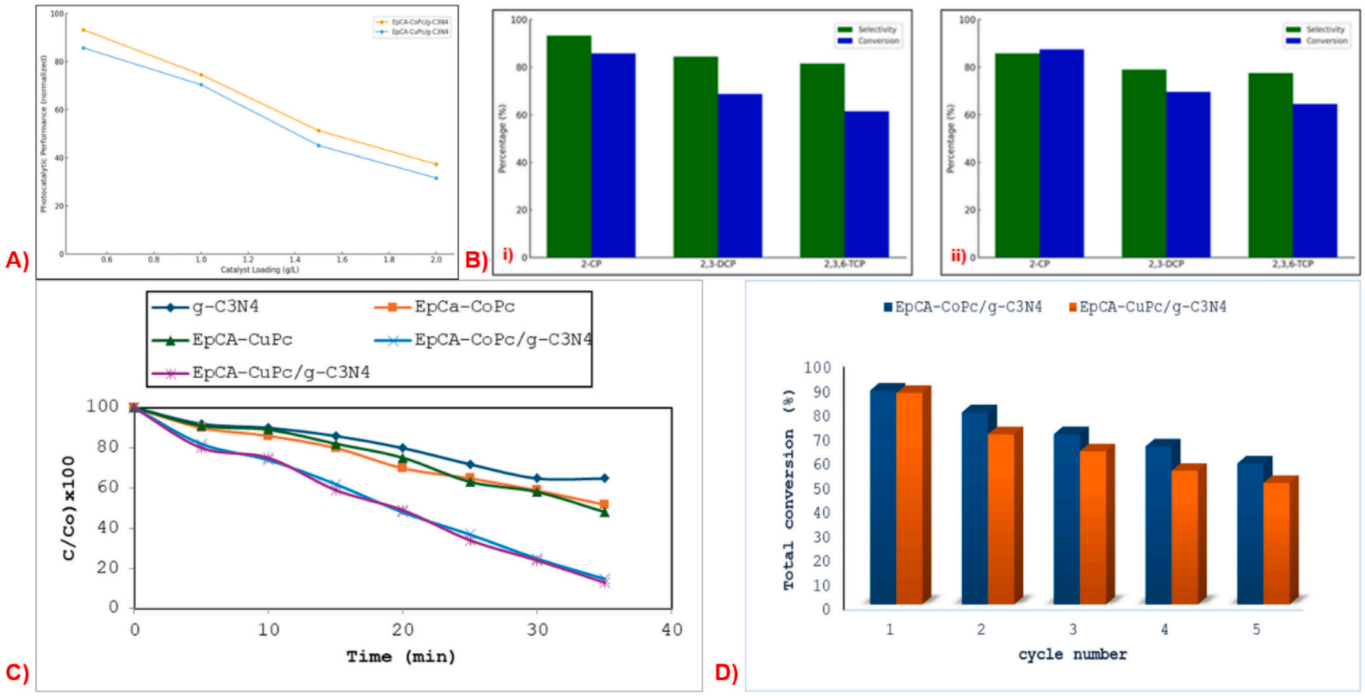


Fig. 4. A) Effect of catalyst loading on the photocatalytic performance of EpCA-CoPc/g-C_3N_4 and EpCA-CuPc/g-C_3N_4. B) Photocatalytic selectivity and conversion of i: EpCA-CoPc/g-C_3N_4 ii: EpCA-CoPc/g-C_3N_4 for chlorophenol derivatives [Pollutant concentration $1{,}2 \times 10^{-5}$ M, optimum loading was determined to be 0.5 g/L for both photocatalysts (25 mg of phthalocyanine in 50 ml ethanol)].C) Time-dependent photocatalytic degradation ($C/C_o \times 100$) of chlorophenols over different catalysts from this work [Pollutant concentration $1{,}2 \times 10^{-5}$ M, optimum loading was determined to be 0.5 g/L for both photocatalysts (25 mg of phthalocyanine in 50 ml ethanol), reaction time: half an hour]. D) Recycling studies of Ep-CA-CoPc/g-C_3N_4 and EpCA-CuPc/g-C_3N_4 [Pollutant concentration $1{,}2 \times 10^{-5}$ M, optimum loading was determined to be 0.5 g/L for both photocatalysts (25 mg of phthalocyanine in 50 ml ethanol), reaction time: half an hour].

Table 1
All photocatalytic results with both catalysts for chlorophenols degradation.

Photocatalyst	Pollutant	Product[a]	Product Selectivity[b](%)	Total Conversion (%)
EpCA-CoPc/g-C_3N_4	2-CP	2-Chloro-1,4-BQ	93.2	85.8
EpCA-CuPc/g-C_3N_4	2-CP	2-Chloro-1,4-BQ	85.8	87.4
EpCA-CoPc/g-C_3N_4	2,3-DCP	2,3-Dichloro-1,4-BQ	84.4	68.7
EpCA-CuPc/g-C_3N_4	2,3-DCP	2,3-Dichloro-1,4-BQ	79.0	69.6
EpCA-CoPc/g-C_3N_4	2,3,6-TCP	2,3,6-Trichloro-1,4-BQ	81.4	61.4
EpCA-CuPc/g-C_3N_4	2,3,6-TCP	2,3,6-Trichloro-1,4-BQ	77.5	64.5
g-C_3N_4	2-CP, 2,3-DCP, 2,3,6-TCP	BQ derivatives	~65	≥58.0
EpCA-CoPc	2-CP, 2,3-DCP, 2,3,6-TCP	BQ derivatives	>52	≥62.0
EpCA-CuPc	2-CP, 2,3-DCP, 2,3,6-TCP	BQ derivatives	>48	≥60.0
Absence of cat.	2-CP, 2,3-DCP, 2,3,6-TCP	BQ derivatives	>25	≥25.0
Absence of light	2-CP, 2,3-DCP, 2,3,6-TCP	BQ derivatives	>10	≥10

[a] : Major product, [b]:Selectivity of benzoquinone derivatives, pollutant concentration $1{,}2 \times 10^{-5}$ M, optimum loading was determined to be 0.5 g/L for both photocatalysts (25 mg of phthalocyanine in 50 ml ethanol).

withdrawing electron density from the π-system and increasing the compound's chemical stability [23]. As the degree of chlorination increases, the aromatic ring becomes increasingly electron-deficient, which significantly enhances its resistance to oxidative attack and slows the overall reaction kinetics. Consequently, highly chlorinated molecules like 2,3,6-trichlorophenol exhibit much greater persistence compared to mono-chlorinated analogs like 2-chlorophenol, which are more susceptible to the initial stages of photocatalytic degradation [24]. Furthermore, the degradation rate is heavily influenced by the mesomeric effect (+M) and the specific radical-mediated pathways facilitated by the photocatalyst. While chlorine is inductively electron-withdrawing, it can partially donate electron density via resonance in the ortho and para positions, thereby facilitating the oxidation of derivatives like 2-chlorophenol [25]. The photocatalytic process is driven primarily by highly reactive superoxide ($O_2^{\bullet-}$) and hydroxyl (•OH) radicals, which initiate a sequence of hydroxylation and dechlorination that transforms these toxic pollutants into less harmful benzoquinone derivatives. The superior performance of EpCA-CoPc/g-C_3N_4 compared to EpCA-CuPc/g-C_3N_4 suggests that the efficiency of the metal center's redox cycle (Co^{2+}/Co^{3+}) plays a critical role in accelerating these charge-transfer processes, thereby dictating the varying rates of mineralization across different phenolic compounds. In this study, both catalysts catalyzed 2-chlorophenol with high selectivity and product conversions, and the oxidation resulted in the formation of 2-chloro-1,4-benzoquinone. The order of highest product conversions for the pollutants was as follows; 2-chlorophenol>2,3-dichlorophenol>2,3,6-trichlorophenol.

Looking at Table 1, the highest product selectivity and conversion rate was obtained in the oxidation of 2-chlorophenol with the EpCA-CoPc/g-C_3N_4 catalyst (93.2% selectivity, 85.8% conversion). The lowest product selectivity was determined as 77.5% in the oxidation of 2,3,6-trichlorophenol with the EpCA-CuPc/g-C_3N_4 catalyst (Fig. 4B). CoPc systems are known from previous studies to generally yield slightly higher selectivity than CuPc [26–31] because the redox cycle (Co^{2+}/Co^{3+}) of the Co center is more efficient in electron transfer. The results in Table 1 also demonstrate the importance of light, the catalyst, and g-C_3N_4 in the degradation of pollutants. One of our objectives in this study is to use photocatalysts to degrade harmful or persistent chlorophenols into less toxic and more environmentally friendly products under mild conditions. These pollutants can generally be efficiently oxidized or reduced using photocatalysts. It was calculated that the EpCA-CoPc/g-C_3N_4 catalyst degaraded 2-chlorophenol by approximately 86%, while the EpCA-CuPc/g-C_3N_4 catalyst degaraded 2-chlorophenol by approximately 87% (Fig. 4C).

In light of studies in the literature, the photocatalytic oxidation mechanisms of chlorophenols, including 2-chlorophenol (2-CP), 2,3-dichlorophenol (2,3-DCP), and 2,3,6-trichlorophenol (2,3,6-TCP), proceed via a general radical-mediated mechanism under irradiation in the presence of photocatalysts such as TiO_2, g-C_3N_4, or phthalocyanine-based materials [32–34]. Upon photon absorption, the photocatalyst produces electron–hole pairs (e^-/h^+), which react with water and molecular oxygen to produce highly reactive species, notably hydroxyl radicals (**•OH**) and superoxide radicals ($\mathbf{O_2^{\bullet-}}$).

$$\text{Catalyst} + h\nu \rightarrow e^-_{CB} - + h^+_{VB}$$

- CB = conduction band (electron)
- VB = valence band (hole)

$$h^+ + H_2O \rightarrow \cdot OH + H^+.$$
$$e^- + O_2 \rightarrow O_2^{\bullet-} + e^-$$

- Hydroxyl radicals (**•OH**): very strong oxidants
- Superoxide radicals ($\mathbf{O_2^{\bullet-}}$): initiate electron transfer and partial oxidation

These radicals attack the aromatic ring of chlorophenols, initiating hydroxylation and consecutive dechlorination, and forming dihydroxy intermediates such as catechol and hydroquinone derivatives; The degree of chlorination affects the site and rate of radical attack. Dihydroxy intermediates are further oxidized by holes or superoxide radicals to form quinone species, including 1,2- and 1,4-benzoquinones. Subsequent attack by hydroxyl radicals causes ring scission, which leads to the formation of small carboxylic acids such as maleic, fumaric, and oxalic acids. Finally, continued oxidation mineralizes these acids to carbon dioxide, water, and chloride ions. For all chlorophenols, the combined effects of hydroxyl radicals, photogenerated holes, and superoxide radicals enable stepwise hydroxylation, dechlorination, quinone formation, ring scission, and complete mineralization, effectively reducing the toxicity of both the parent compounds and their intermediates [35–39]. In this study, benzoquinone derivatives were identified as the major products for all three chlorophenols.

Photocatalyst recycling studies are crucial for both environmental sustainability and economic efficiency. Because photocatalysts typically contain expensive metal centers or complex composite structures, their reusability after each reaction significantly reduces costs. Furthermore, maintaining the catalyst's structural stability and photochemical activity increases system reliability in long-term applications. In our recycling studies, we aimed to highlight the durability and reusability of the photocatalysts we used by determining whether the catalysts exhibited any performance loss when reused. In our study, both catalysts achieved over 50% total product conversion after 5 cycles, demonstrating that they maintained their activity and durability after 5 cycles. The most striking result from the recycling studies was that the EpCA-CoPc/g-C_3N_4 catalyst achieved approximately 65% total product conversion after 4 cycles, and the EpCA-CuPc/g-C_3N_4 catalyst achieved approximately 63% total product conversion after 3 cycles (Fig. 4D).

The effects of different scavengers on the photocatalytic activity are

summarized in Table 2. In the absence of any scavenger, the photocatalytic system exhibited the highest degradation efficiency, indicating an unhindered reaction pathway. The introduction of isopropanol (IPA), a well-known hydroxyl radical (•OH) scavenger, resulted in a marked suppression of photocatalytic activity, underscoring the significant involvement of •OH radicals in the degradation process. Notably, the most pronounced inhibition was observed upon the addition of p-benzoquinone (BQ), suggesting that superoxide radicals ($O_2^{\bullet-}$) play a predominant role in the photocatalytic reaction. In contrast, the presence of EDTA-2Na led to a moderate decrease in activity, indicating that photogenerated holes (h^+) act as contributing, but not dominant, reactive species. Meanwhile, the addition of sodium azide (NaN_3), a singlet oxygen ($^1O_2$) scavenger, caused only a slight or negligible reduction in photocatalytic efficiency, implying a limited contribution of $^1O_2$. Taken together, these observations provide compelling, albeit indirect, evidence that the photocatalytic process is predominantly driven by $O_2^{\bullet-}$ and •OH-mediated pathways, in good agreement with the proposed reaction mechanism.

Over the last 10 years, there are many articles in the literature in which phthalocyanine and grafitic carbon nitride derivative materials are prepared in combination and their use in different application areas is investigated [45–54]. A very limited number of studies are only on the removal of phenolic or dye compounds [40–42]. A summary of the studies on ZnPc, CoPc, FePc and NiPc incorporated into g-C_3N_4 matrices is given in Table 3 [43,44,55–57]. Zada et al. reported that ZnPc/g-C_3N_4 catalyzed the degradation of 2,4-DCP up to 85–90% in 120 min under visible light [43]. Wang et al. reported that in the presence of CoPc/g-C_3N_4, 2,4-DCP was degraded up to approximately 80% in only 90 min under visible light [44]. This study highlights the effect on catalytic activity in the presence of phthalocyanines with redox active metal centers. Li and colleagues reported that the addition of g-C_3N_4 to a FePc/CeO_2 heterojunction resulted in approximately 90% degradation of 2,4-dichlorophenol in 60 min [55]. Khan and colleagues reported that 80% degradation of 4-chlorophenol was observed in the presence of NiPc/g-C_3N_4 photocatalyst in 60 min [56]. Considering that the degradation rates of 2,4-dichlorophenol and 4-chlorophenol were in the range of 45–60% in photocatalytic studies with bare g-C_3N_4 [57], it is clear that the presence of phthalocyanines in the catalytic system is remarkably important. Phthalocyanines increase visible light absorption and facilitate electron-hole separation, promoting the formation of superoxide radicals ($O_2^{\bullet-}$), vacancies (h^+), and sometimes singlet oxygen ($^1O_2$), which are responsible for oxidative degradation. A review of the literature in Table 3 reveals that studies on various and highly chlorinated phenol compounds are limited. Furthermore, the lack of sufficient data on photostability, recyclability, and by product identification in these important studies is a significant shortcoming.

Table 2
Effect of radical scavengers on the photocatalytic performance.

Scavenger	Reactive species	Effect on photocatalytic activity	Results
None (control)	–	Highest degradation efficiency	Normal photocatalytic process
Isopropanol (IPA) / tert-Butanol	•OH (hydroxyl radicals)	Significant decrease	•OH radicals play an important role
p-Benzoquinone (BQ)	$O_2^{\bullet-}$ (superoxide radicals)	Strong inhibition	$O_2^{\bullet-}$ is a dominant reactive species
EDTA-2Na	h^+ (photogenerated holes)	Moderate decrease	h^+ contributes as a secondary active species
Sodium azide (NaN_3)	$^1O_2$ (singlet oxygen)	Slight or negligible decrease	$^1O_2$ plays a minor role

3.3. Theoretical calculations

The relative positions of the HOMO and LUMO levels play a key role in determining the optoelectronic behavior of molecular systems and provide valuable insight into the degradation pathways of environmentally hazardous compounds. In addition, these energy levels are closely associated with fundamental properties such as band gap magnitude, molecular reactivity, and kinetic stability. In this study, the molecular orbitals and corresponding electron density distributions of compounds CoPc and CuPc (Fig. 5a-d), as well as g-C_4N_3, 2-chlorophenol, 2,3-Dichlorophenol and 2,3,6-trichlorophenol, were obtained using DFT calculations with the B3LYP functional and the LanL2DZ basis set. These calculations were carried out to achieve a deeper understanding of the photodegradation mechanism of 2-chlorophenol, 2,3-Dichlorophenol and 2,3,6-trichlorophenol. The calculated HOMO-LUMO energy band gaps were found to be 2.20 eV for CoPc, 2.15 eV for CuPc, 4.24 eV for g-C_4N_3, 5.80 eV for 2-chlorophenol, 5.82 eV for 2,3-Dichlorophenol and 5.77 eV 2,3,6-trichlorophenol (Fig. 5e). For both phthalocyanine derivatives, the HOMO electron density is predominantly concentrated on the macrocyclic core, while the LUMO orbitals are distributed over the same region with comparatively lower electron density. The LUMO energy levels were determined as −3.07 eV, −3.13 eV, −3.11 eV, −0.75, −1.05 and − 1.39 eV for CoPc, CuPc, g-C_4N_3, 2-chlorophenol, 2,3-Dichlorophenol and 2,3,6-trichlorophenol, respectively. These DFT-derived LUMO values strongly support the proposed degradation pathway: upon light irradiation, photoexcited electrons in g-C_4N_3 are transferred to the phthalocyanine system, react with water and molecular oxygen to produce highly reactive species, notably hydroxyl radicals and superoxide radicals, ultimately leading to decomposition of chlorophenols. As the number of chlorine atoms in the molecule increases with and polarization effects caused by the chlorine substituent, the π-electron delocalization in the aromatic ring deteriorates, which reduces the electron density in the hydroxyl group, leading to a decrease in the decomposition rate [58]. In other words, an increase in the number of chlorine atoms causes a decrease in the decomposition rate. In addition, a molecule with a larger energy band gap is less reactive, which tend to be more stable because they are less susceptible to reduction or oxidation [59]. According to DFT results, the reason why 2-chlorophenol has a higher removal efficiency may be due to its smaller band gap in comparison with 2,3-Dichlorophenol and 2,3,6-trichlorophenol.

3.4. Proposed reaction mechanism

The synthesis and characterization of g-C_3N_4 have been extensively investigated and comprehensively reported in numerous studies in the literature. [6,60–63]. According to previous studies, the C 1 s spectrum of pristine g-C_3N_4 typically exhibits a peak at approximately 284.2 eV attributed to graphitic C—C bonds, while the peak located at around ~285.6 eV corresponds to N–C=N bonds originating from heptazine units [63]. In the N 1 s spectrum, the peak at ~399.9 eV is assigned to sp^2-hybridized C–N=C species, whereas the peak observed at approximately ~401.0 eV is associated with bridging or graphitic nitrogen species [64–66]. Upon the formation of composites with metal phthalocyanine derivatives, slight shifts in the binding energies of these characteristic C 1 s and N 1 s peaks are observed, indicating pronounced electronic interactions between g-C_3N_4 and the metal phthalocyanine components. Such binding energy shifts, particularly in the N 1 s region, have been widely reported as a signature of interfacial charge redistribution in heterojunction systems [67,68]. The extended π-conjugated structures and central metal ions of metal phthalocyanines enable effective interaction with the lone-pair-electron-rich nitrogen species of g-C_3N_4, facilitating interfacial transfer of photogenerated electrons and suppressing charge recombination [69,70].

The general reaction mechanism proposed for photooxidation reactions of organic pollutants can be explained by the oxidationof organic

Table 3
A summary of the studies on ZnPc, CoPc, FePc and NiPc incorporated into g-C_3N_4 matrices.

Photocatalyst System	Pollutant	Light Conditions	Degradation Efficiency / Time	Mechanism	Ref.
ZnPc/g-C_3N_4 nanocomposite[a]	2,4-DCP	Visible light ($\lambda > 420$ nm)	≈ 85% degradation in 120 min	$O_2^{\bullet-}$ and h^+ are the main reactive species; enhanced charge separation and extended visible absorption	[40]
CoPc/g-C_3N_4 composite[b]	2,4-DCP	Visible light ($\lambda > 400$ nm)	≈ 78% degradation in 90 min	$O_2^{\bullet-}$ and $^1O_2$ are key species; improved electron transfer but slightly lower stability	[41]
FePc/CeO_2/g-C_3N_4[c]	2,4-DCP	Visible light (450 nm LED)	≈ 90% degradation in 100 min	*Z*-scheme charge transfer; h^+ and $O_2^{\bullet-}$ are dominant	[42]
NiPc/g-C_3N_4[d]	4-CP	Visible light ($\lambda > 420$ nm) + H_2O_2	≈ 80% degradation in 60 min	•OH and $O_2^{\bullet-}$ radicals dominate; narrowed band gap and improved photoresponse	[43]
bare g-C_3N_4[e]	2,4-DCP, 4-CP	Visible light	≈ 45–60% degradation	Fast charge recombination; limited visible-light absorption	[44]

[a] Zn-phthalocyanine/g-C_3N_4 nanocomposite, [b]Co-phthalocyanine/g-C_3N_4 composite, [c]Fe-phthalocyanine/g-C_3N_4 Z-scheme heterostructure, [d]Ni-phthalocyanine/g-C_3N_4, [e]non-phthalocyanine/ g-C_3N_4. 2,4-DCP: 2,4-Dichlorophenol, 4-CP:4-Chlorophenol.

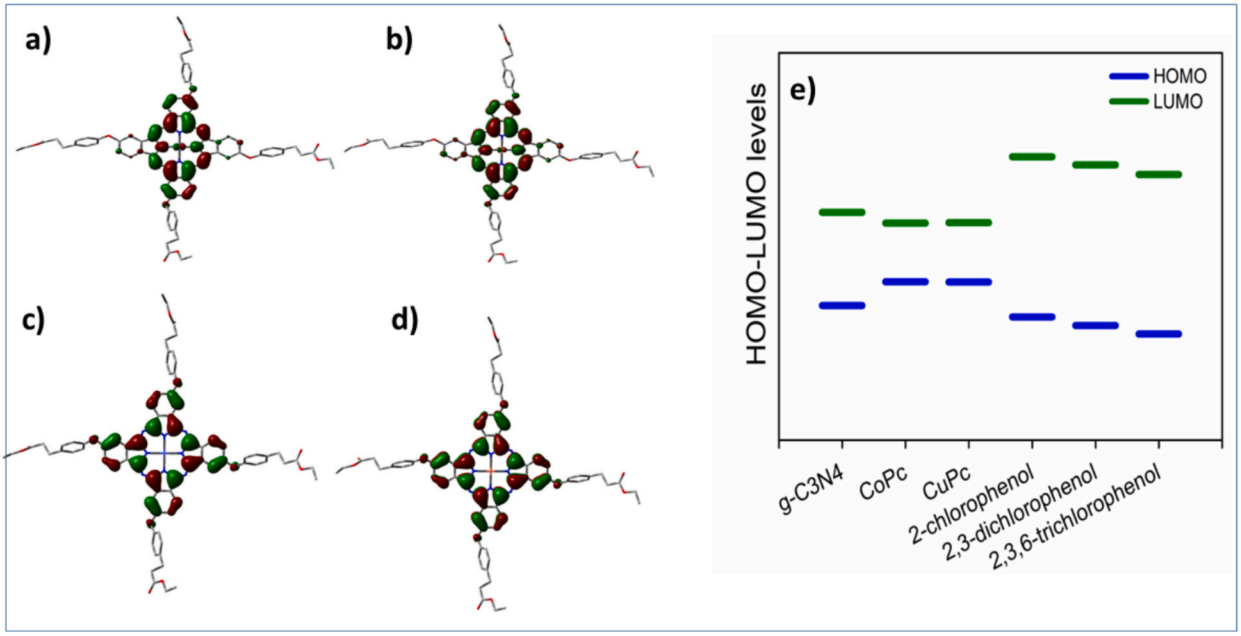


Fig. 5. HOMO a), b) and LUMO c), d) energy levels of CoPc, CuPc and e) HOMO-LUMO energy levels of g-C_3N_4, EpCA-CoPc, EpCA-CuPc, 2-chlorophenol, 2,3-Dichlorophenol and 2,3,6-trichlorophenol.

pollutants into less harmful, less toxic and small molecules. During the reaction, active species can be formed by electron transfer from the valence band (VB) to the HOMO (the highest occupied molecular orbital) and then from the LUMO (The lowest unoccupied molecular orbital) to the conduction band (CP). Due to the low energy of the conduction band of g-C_3N_4, electron transfer easily occurs from this band to the HOMO of metal phthalocyanine. Moreover, the excited electrons in the LUMO of metal phthalocyanine flow to the valence band (VB) of C3N4. This electron filled in the conduction band reacts with dissolved oxygen to form superoxide radical ions ($\mathbf{O_2^{\bullet-}}$) [6,63]. Then, due to these radicals are more active species, they cause to decompose the organic pollutant to less harmful small molecules [64,65] (Fig. 6).

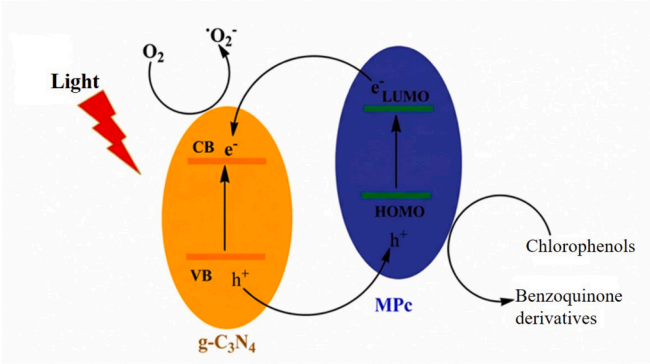


Fig. 6. Proposed mechanism for the photocatalytic degradation of chlorophenols over the g-C_3N_4/MPc heterojunction [MPc: EpCA-CoPc and EpCA-CuPc].

4. Conclusion

In conclusion, this work demonstrated that EpCA-CoPc/g-C_3N_4 and EpCA-CuPc/g-C_3N_4 photocatalysts exhibit high photocatalytic efficiency and stability in the degradation of chlorophenols under visible light irradiation. The optimum catalyst loading was determined as 0.5 g/L, providing a balance between active surface area and light utilization efficiency. Both catalysts effectively degraded 2-chlorophenol, 2,3-dichlorophenol, and 2,3,6-trichlorophenol through radical-mediated oxidation pathways, with benzoquinone derivatives identified as the main intermediates. Among the tested systems, EpCA-CoPc/g-C_3N_4 showed superior activity and selectivity (85.8% conversion, 93.2%

selectivity for 2-chlorophenol), attributed to the efficient Co^{2+}/Co^{3+} redox cycle facilitating charge transfer. Recycling experiments confirmed the durability of both photocatalysts, maintaining over 50% of their activity after five cycles. This specific design effectively disrupts the interlayer stacking of g-C_3N_4, leading to superior textural properties—such as increased BET surface area and pore volume—which facilitate enhanced mass transport and active site accessibility compared to pristine g-C_3N_4. Furthermore, while existing research frequently lacks sufficient data on complex pollutants and stability, this method demonstrates high efficiency in degrading highly chlorinated compounds like 2,3,6-trichlorophenol and provides comprehensive evidence regarding photostability, recyclability, and the identification of benzoquinone derivatives as major oxidation products. Computational studies on these structures further corroborate the experimental results.

This approach provides a novel perspective on environmental sustainability and cost-effectiveness by integrating green chemistry principles with efficient materials engineering. The selection of ethyl p-coumarate (EpCA)—a derivative of the naturally occurring p-coumaric acid—as a peripheral substituent offers a non-toxic, bio-inspired alternative to traditional synthetic groups, while the use of earth-abundant cobalt and copper instead of noble metals significantly reduces both the economic burden and the environmental footprint. From a manufacturing standpoint, the utilization of non-covalent π-π stacking rather than complex covalent grafting strategies streamlines the synthesis process, offering a time- and energy-efficient route that leverages inexpensive precursors like urea or melamine for the g-C_3N_4 support. Furthermore, the catalysts' ability to operate under visible light eliminates the need for energy-intensive UV radiation, and their demonstrated stability over five consecutive cycles ensures a sustainable and economically viable pollution management system for industrial-scale applications.

CRediT authorship contribution statement

Cagla Akkol: Writing – review & editing, Writing – original draft, Visualization, Validation, Software, Resources, Investigation, Funding acquisition, Formal analysis, Data curation, Conceptualization. **Ece Tugba Saka:** Writing – review & editing, Writing – original draft, Visualization, Validation, Supervision, Software, Resources, Project administration, Methodology, Investigation, Funding acquisition, Formal analysis, Data curation, Conceptualization. **Ahmet Senocak:** Formal analysis, Investigation, Methodology, Writing – original draft.

Declaration of competing interest

The authors declare that they have no known competing financial interests or personal relationships that could have appeared to influence the work reported in this paper.

Acknowledgment

This study was supported by The Research Fund of Karadeniz Technical University (Project no: 16562) Trabzon, Turkiye.

Appendix A. Supplementary data

Supplementary data to this article can be found online at https://doi.org/10.1016/j.inoche.2026.116457.

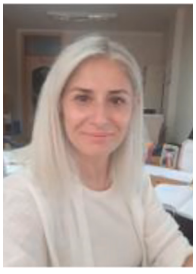
Data availability

The datasets used and/or analyzed during the current study are available from the corresponding author on reasonable request.

References

[1] P.K. Arora, H. Bae, Bacterial degradation of chlorophenols and their derivatives, Microb. Cell Fact. 13 (2014) 31.
[2] A. Farrell, B. Quilty, The enhancement of 2-chlorophenol degradation by a mixed microbial community when augmented with *pseudomonas putida* CP1, J. Ind. Microbiol. Biotechnol. 28 (2002) 316–324.
[3] E. Schmidt, M. Hellwig, H.-J. Knackmuss, Degradation of mono-chlorophenols by a mixed microbial community via a meta-cleavage pathway, Appl. Environ. Microbiol. 46 (1983) 1038–1044.
[4] Agency for Toxic Substances and Disease Registry (ATSDR), in: U.S. Department of Health and Human Services (Ed.), Toxicological Profile for Chlorophenols, 2008.
[5] International Programme on Chemical Safety, Chlorophenols (Environmental Health Criteria 93), World Health Organization, Geneva, 1989.
[6] X. Wang, K. Maeda, A. Thomas, K. Takanabe, G. Xin, J.M. Carlsson, K. Domen, M. Antonietti, A metal-free polymeric photocatalyst for hydrogen production from water under visible light, Nat. Mater. 8 (2009) 76–80.
[7] G. Dong, L. Zhang, D. Chen, Synthesis and modification of graphitic carbon nitride for improved photocatalytic performance, J. Photochem. Photobiol. C 22 (2015) 3–28.
[8] W.-J. Ong, L.-L. Tan, Y.H. Ng, S.-T. Yong, S.-P. Chai, Graphitic carbon nitride (g-C_3N_4)-based photocatalysts for artificial photosynthesis and environmental remediation: a review, Chem. Rev. 116 (2016) 7159–7329.
[9] J. Zhang, Y. Chen, X. Wang, Two-dimensional g-C_3N_4 nanosheets for high-performance photocatalysis, Energ. Environ. Sci. 8 (2015) 3092–3108.
[10] K. Maeda, K. Domen, Photocatalytic water splitting: recent progress and future challenges, J. Phys. Chem. Lett. 1 (2010) 2655–2661.
[11] X. Zhang, X. Xie, H. Wang, J. Zhang, B. Pan, Y. Xie, Enhanced visible-light photocatalytic activity of graphitic carbon nitride via coupling with cobalt phthalocyanine, Nanoscale 5 (2013) 2274–2282.
[12] D. Jiang, P. Xu, H. Wang, X. Bai, L. Wang, Construction of cu-phthalocyanine/g-C_3N_4 heterostructures for boosted visible-light photocatalysis via efficient charge separation, Appl. Catal. Environ. 250 (2019) 322–330.
[13] T. Xiong, W. Cen, Y. Zhang, L. Ding, W. Chen, Metal phthalocyanine-modified carbon nitride for improved visible-light-driven photocatalytic reactions: synergistic effects of π–π conjugation and metal-centered redox activity, Chem. Eng. J. 381 (2020) 122641.
[14] A. Fujishima, X. Zhang, D.A. Tryk, TiO_2 photocatalysis and related surface phenomena, Surf. Sci. Rep. 63 (2008) 515–582.
[15] M.R. Hoffmann, S.T. Martin, W. Choi, D.W. Bahnemann, Environmental applications of semiconductor photocatalysis, Chem. Rev. 95 (1995) 69–96.
[16] E.T. Saka, A. Senocak, C. Akkol, Synthesis of phthalocyanine/C3N4 structures and investigation of photocatalytic activities in the oxidation reaction of 4-nitrophenol, Journal of Coordination Chemistry 78 (2024) 31–43.
[17] A. Mills, S. Le Hunte, An overview of semiconductor photocatalysis, J. Photochem. Photobiol. A Chem. 108 (1997) 1–35.
[18] C. Kittel, Introduction to Solid State Physics, 8th ed., Wiley, 2005.
[19] W. Li, S. Yuan, J. Sun, Q. Li, W. Jiang, J. Cao, Ethyl p-coumarate exerts antifungal activity in vitro and in vivo against *Alternaria alternata* via membrane-targeted mechanism, Int. J. Food Microbiol. 278 (2018) 26–35.
[20] L. Dong, et al., Synergistic multiple active species for the photocatalytic performance of g-C_3N_4-IMA-$FePcCl_{16}$ under visible light, Chem. Eng. J. 365 (2019) 288–297.
[21] G. Zhang, et al., Synergistic photocatalytic properties and mechanism of g-C_3N_4 coupled with zinc phthalocyanine under visible-light irradiation, Inorg. Chem. 61 (2022) 8935–8944.
[22] D. Akyüz, et al., G-C_3N_4/polymeric metallophthalocyanine as novel composite electrocatalysts, J. Power Sources 597 (2024) 233343.
[23] J.C. D'Oliveira, G. Al-Sayyed, P. Pichat, Photodegradation of 2-chlorophenol, 3-chlorophenol and 4-chlorophenol in TiO2 aqueous suspensions: detoxicity, intermediates and precursor-product relationships, J. Photochem. Photobiol. A Chem. 72 (3) (1993) 261–271.
[24] C. Minero, G. Mariella, V. Maurino, E. Pelizzetti, Photocatalytic transformation of organic compounds in the presence of inorganic ions. 2. Competitive reactions of phenol and alcohols on a titanium dioxide−fluoride system, Langmuir 16 (6) (2000) 2632–2641.
[25] R. Vinu, G. Madras, Photocatalytic degradation of phenolics using TiO2 and ag-substituted polyoxometalate, Chem. Eng. J. 147 (2009) 282–293.
[26] E.T. Saka, Z. Bıyıklıoğlu, H. Kantekin, Microwave-assisted synthesis and characterization of co(II) phthalocyanine and its catalytic activity on 4-nitrophenol oxidation, Turk. J. Chem. 38 (2014) 1166–1173.
[27] E.T. Saka, H. Kantekin, Z. Bıyıklıoğlu, Facile synthesis of highly active co(II) and Fe (II) phthalocyanine catalysts for aerobic oxidation of phenolic compounds, Journal of Coordination Chemistry 68 (2015) 1132–1141.
[28] E.T. Saka, D. Çakır, Z. Bıyıklıoğlu, H. Kantekin, New soluble peripherally tetra-substituted co(II), Fe(II) phthalocyanines: synthesis, spectroscopic characterization and catalytic activity in cyclohexene oxidation, Dyes Pigments 98 (2013) 255–262.
[29] E.T. Saka, Z. Bıyıklıoğlu, H. Kantekin, İ. Kani, Synthesis, characterization and catalytic activity of peripherally tetra-substituted co(II) phthalocyanines for cyclohexene oxidation, Appl. Organomet. Chem. 27 (2013) 59–67.
[30] E.T. Saka, E. Dugdu, Y. Ünver, Degradation of substituted phenols with different oxygen sources catalyzed by Co(II) and Cu(II) phthalocyanine complexes, J. Coord. Chem. 72 (2019) 1589461.
[31] E.T. Saka, İ. Acar, Z. Bıyıklıoğlu, H. Kantekin, A. Aktas, Investigation of catalytic activity of new co(II) phthalocyanine complexes in cyclohexene oxidation using different oxidants, J. Organomet. Chem. 745–746 (2013) 18–24.

[32] M. Pera-Titus, V. García-Molina, M.A. Baños, J. Giménez, S. Esplugas, Degradation of chlorophenols by means of advanced oxidation processes: a general review, Appl. Catal. Environ. 47 (2004) 219–256.
[33] X. Li, G. Chen, L. Yang, Z. Jin, Photocatalytic degradation of 2-chlorophenol by g-C_3N_4 under visible light irradiation: reaction mechanism and pathway, Sep. Purif. Technol. 178 (2017) 122–130.
[34] W. Li, X. Yu, J. Zeng, P. Wang, X. Wang, Enhanced visible-light degradation of chlorophenols by metal-phthalocyanine–sensitized photocatalysts: mechanism and reactive species, J. Photochem. Photobiol. A Chem. 361 (2018) 34–43.
[35] Z. Guo, X. Xu, Y. Liu, et al., Photocatalytic degradation of chlorophenols in aquatic environments: mechanisms, kinetics, and influencing factors, J. Environ. Manage. 321 (2022) 114822.
[36] R. Wu, L. Zhou, J. Chen, et al., Visible-light-driven degradation of chlorophenols via advanced photocatalytic systems, RSC Adv. 13 (2023) 7570–7582.
[37] A. Suri, I. Singh, Oxidation pathways of chlorophenols by heterogeneous photocatalysts: environmental implications, J. Environ. Manage. 146 (2014) 213–222.
[38] S. Esplugas, J. Giménez, S. Contreras, E. Pascual, M. Rodríguez, Degradation of chlorophenols by means of advanced oxidation processes: a review, J. Environ. Sci. Health A 41 (2006) 1659–1673.
[39] M. Priyadarshini, K. Patel, S. Patel, Photocatalytic degradation of halogenated phenols: mechanistic insights and catalyst design strategies, Environ. Sci. Pollut. Res. 31 (2024) 11857–11872.
[40] X. Lu, Y. Wang, L. Chen, Q. Zhang, Enhanced visible-light degradation of 4-chlorophenol over Zn-phthalocyanine modified g-C_3N_4, Inorg. Chem. Commun. 118 (2020) 108019.
[41] J. Xu, S. Zhao, H. Li, Z. Chen, Zn-tetracarboxyphthalocyanine/g-C_3N_4 nanofiber composites for photocatalytic degradation of chlorinated phenols under visible light, Inorganic Chemistry Communications 70 (2016) 43–48.
[42] S. Bakhtiar, M. Khan, R. Ullah, S. Ali, Zn-phthalocyanine sensitized g-C_3N_4 for visible-light photocatalysis of 2,4-dichlorophenol, Inorganic Chemistry Communications 150 (2023) 110643.
[43] A. Zada, Y. Dong, X. Fu, Zinc phthalocyanine-sensitized g-C_3N_4 photocatalyst for enhanced visible-light degradation of chlorophenols, Appl. Catal. Environ. 298 (2021) 120541.
[44] L. Wang, Y. Zhang, J. Liu, Cobalt phthalocyanine modified g-C_3N_4 for visible-light degradation of chlorophenols, J. Mol. Catal. A Chem. 432 (2022) 112736.
[45] G. Liu, Z. Li, G. Wang, et al., Phosphorous-doped g-C_3N_4 supported cobalt phthalocyanine for efficient CO_2 reduction under visible light, Chem. Phys. 559 (2021) 112564.
[46] S.U.H. Bakhtiar, A. Zada, F. Raziq, et al., Zinc phthalocyanine sensitized g-C_3N_4 photocatalyst for exceptional photocatalytic hydrogen evolution and pollutant degradation, Int. J. Hydrogen Energy 48 (2023) 16320–16329.
[47] H. Li, H. Liu, Y. Shu, et al., Polymeric cobalt phthalocyanine@mesoporous g-C_3N_4 composite for efficient photocatalytic CO_2 reduction, J. Mater. Chem. A 9 (2021) 12057–12064.
[48] C. Chu, M. Ding, Y. Su, et al., Polymeric iron phthalocyanine/g-C_3N_4 composite catalyst by mechanical force enhanced stripping and recombination for solar-induced contaminant degradation and CO_2 reduction, Appl. Catal. Environ. 305 (2022) 121119.
[49] J. Sun, W. Lin, L. Ma, et al., Efficient photocatalytic conversion of CO_2 on ultrathin metal phthalocyanine/g-C_3N_4 heterojunctions by promoting charge transfer, J. Catal. 389 (2020) 369–377.
[50] M.K.T. Chee, T. Tan, S. Li, et al., Insights into zinc phthalocyanine as a photosensitizer for amorphous carbon nitride, ACS Appl. Energy Mater. 6 (2023) 1045–1055.
[51] N. Nataraj, D.P. Jaihindh, S. Chen, A. Sabbah, S. Muthusamy, S. Devi, Y.-F. Lin, A. Mahalingam, Substitution-functionalized copper phthalocyanine (CuPc)/carbon nitride (g-C_3N_4) electrocatalysts for the simultaneous detection of 4-nitroaniline and nitrofurantoin, environmental science: nano 12 (2025) 3731–3746.
[52] E.T. Saka, et al., Synthesis of phthalocyanine/C_3N_4 structures and their catalytic activity, J. Coord. Chem. 77 (2024) 2400573.
[53] X. Zhang, et al., Visible/near-infrared-light-induced H_2 production over g-C_3N_4/polymeric iron phthalocyanine composites, ChemSusChem 8 (2015) 3124–3132.
[54] J. **Qian,** Y. Liu, W. Zheng, B. Zhou, X. Dong X. Covalent modification of iron phthalocyanine into the skeleton of graphitic carbon nitride for enhanced visible-light photocatalytic reduction of nitroaromatic compounds. Catalysts 12 (2022) 752.
[55] H. Li, P. Zhou, S. Wu, Fe-phthalocyanine/CeO_2 heterojunction with g-C_3N_4 for enhanced chlorophenol photodegradation under visible light, Dalton Trans. 53 (2024) 6123–6135.
[56] R. Khan, M. Akhtar, R. Nazir, Ni-phthalocyanine/g-C_3N_4 composite for visible-light assisted degradation of chlorophenols, J. Photochem. Photobiol. A Chem. 442 (2023) 114986.
[57] M. Sun, Y. Liu, Advances in photocatalytic degradation of chlorophenols using phthalocyanine-modified g-C_3N_4 systems, RSC Adv. 13 (2023) 17248–17263.
[58] D.J. Morgan, Core-level reference spectra for bulk graphitic carbon nitride (g-C3N4), Surf. Sci. Spectra 28 (2021) 014007.
[59] M. Benedet, G.A. Rizzi, D. Barreca, A. Gasparotto, C. Maccato, XPS analysis of graphitic carbon nitride functionalized with CoO and CoFe2O4, Surface Science Spectra 30 (2023) 014004.
[60] Z. Zazimal, D. Plasienka, S. Atri, L. Vrana, O. Monfort, P. Stavarek, P. Kluson, M. Sob, T. Homola, Unveiling the effect of the polymerization degree of graphitic carbon nitride on the surface functionalization by low-temperature plasma: insights from XPS and DFT study, Appl. Surf. Sci. 699 (2025) 163073.
[61] W.F. Li, Y. Wang, X.Y. Yang, F.Q. Liu, W.H. Li, Graphitic carbon nitride prepared by rapid recrystallization for Photoelectrochemical anticorrosion, ACS Appl. Nano Mater. 2 (2019) 7559-+.
[62] S.T. Mkhondwane, S. Mgidlana, T. Nyokong, Asymmetric phthalocyanine-graphitic carbon nitride nanosheets conjugate on zinc oxide fibers for combined ultrasound and visible light driven degradation of rhodamine 6G, *journal of Photochemistry & Photobiology, a:* Chemistry 447 (2024) 115245.
[63] Y. Zhang, T. Mori, J. Ye, M. Antonietti, Phosphorus-doped carbon nitride solid: enhanced electrical conductivity and photocurrent generation, J. Am. Chem. Soc. 134 (2012) 19326–19329.
[64] G. Dong, Y. Zhang, Q. Pan, J. Qiu, A fantastic graphitic carbon nitride (g-C_3N_4) material: electronic structure, photocatalytic and photoelectronic properties, J. Photochem. Photobiol. C Photchem. Rev. 20 (2014) 33–50.
[65] J. Xu, Y. Wang, Y. Zhu, Enhanced visible-light photocatalytic activity of graphitic carbon nitride through heterojunction construction, Appl. Catal. Environ. 168–169 (2015) 105–112.
[66] J. Liu, T. Zhang, Z. Wang, G. Dawson, W. Chen, Simple pyrolysis of urea into graphitic carbon nitride with recyclable adsorption and photocatalytic activity, J. Mater. Chem. A 5 (2017) 1658–1666.
[67] S. Zhao, S. Chen, H. Yu, X. Quan, Metal phthalocyanine/g-C_3N_4 heterojunctions for enhanced visible-light photocatalytic activity, Appl. Catal. Environ. 224 (2018) 563–572.
[68] X. Chen, J. Li, Z. Pan, Y. Wang, Interfacial charge transfer in phthalocyanine-based heterojunction photocatalysts, Chem. Eng. J. 389 (2020) 124402.
[69] A. Khachay, Understanding the adsorption mechanism of phenol and Para-Chlorophenol onto Sepiolite clay: a combined DFT calculations, molecular dynamics simulations, and isotherm analysis, Water 17 (2025) 1335.
[70] W. Lan, Exploring the activation potential of heme for 2,4-dichlorophenol, 2,4,6-trichlorophenol, and pentachlorophenol, Sci. Rep. 14 (1) (2024) 23212.



Ece Tugba Saka is a Full Professor of Inorganic Chemistry in the Department of Chemistry at Karadeniz Technical University, Turkey. She received her Ph.D. in Inorganic Chemistry from the same institution in 2012. Her academic career is marked by a significant international research presence, including a post-doctoral fellowship at North Carolina State University, USA, supported by the Turkish Research Council (TUBITAK), and teaching mobility at the University of Camerino, Italy. Professor Saka's research focuses on the synthesis and characterization of macrocyclic compounds, with a specific emphasis on phthalocyanines and their applications in homogeneous and heterogeneous catalysis. Her work extensively explores the catalytic oxidation of organic pollutants, phenolic compounds, and the development of light-driven photocatalytic systems for environmental remediation. She has authored over 60 peer-reviewed articles in prestigious journals. Currently, she holds an h-index of 21 with nearly 500 citations (excluding self-citations). In recognition of her scholarly achievements, she was honored with the Young Science and Art People Award in 2018.